Applied Science and Engineering Progress, Vol. 20, No. 2, 2027, 8261

Research Article

Carbonization Effects on the Biaxial Performance of Carbon Fiber Composites

Maximilian Kroll*, Maxime Maghe, Claudia Creighton
Carbon Nexus, Institute for Frontier Materials, Faculty of Science, Engineering and Built Environment, Deakin University, Geelong, Australia

Russell Varley
School of Engineering, RMIT University, Melbourne, Australia

Rostislav Svidler, Lothar Kroll
Department of Lightweight Structures and Polymer Technology, Faculty of Mechanical Engineering, University of Technology Chemnitz, Chemnitz, Germany

* Corresponding author. E-mail: m.kroll@deakin.edu.au DOI: 10.14416/j.asep.2026.07.014
Received: 4 March 2026; Revised: 30 April 2026; Accepted: 13 July 2026; Published online: 27 July 2026.

Abstract
This work represents one of the first attempts to directly link industrially relevant carbonization rates of 50k carbon fiber tows to resulting multiaxial composite performance. Carbonization rates were systematically varied to produce three carbon fiber variants, which were then processed into carbon fiber reinforced polymer (CFRP) laminates and tested under biaxial compression-shear loading using a fixed-clamped Iosipescu configuration. While uniaxial tensile properties of the single carbon fibers differed only marginally, biaxial testing of CFRP revealed differences in peak transverse compressive and shear stresses. CFRP reinforced with fibers carbonized at slow and medium rate retained higher biaxial strength compared to the fastest carbonization condition. The failure morphology evolved from predominantly shear-dominated cracking to mixed shear-splitting behavior and finally to splitting-dominated failure with increased carbonization rate. The results provide a basis for application-oriented carbon fiber manufacturing and for defining acceptable carbonization rates toward more efficient production.

Keywords: Biaxial compression-shear loading, Carbon fiber, Carbon fiber reinforced polymer (CFRP), Carbonization, Puck inter-fiber failure criterion

1 Introduction

PAN-based carbon fibers are indispensable for lightweight structures, yet their broader adoption beyond high-tech markets remains constrained by the inherently complex, energy-intensive, and costly manufacturing process [1]. Life cycle assessments and process analyses identify the thermal conversion steps as the dominant contributors to energy demand, with stabilization and carbonization accounting for over 94 % of energy-related costs and thus representing the primary levers for cost reduction [2]-[5]. Consequently, several approaches have been proposed to increase the efficiency of PAN-based carbon fiber production, including improved oven and furnace design [6], heat recovery [4], [7], precursor and comonomer adaptation [8]-[10], and alternative conversion strategies based on microwave-, plasma-, or laser energy input [11]-[13].

From an industrial perspective, the most attractive efficiency measures are those that can be implemented on existing production lines with minimal additional investment. This makes systematic optimization of process parameters such as temperature, residence times, and tow tension particularly relevant. However, any acceleration of the conversion process must ultimately be evaluated against the property requirements of the final composite application. This is especially important for high-volume sectors such as the automotive industry, where robust laminate performance and damage tolerance are at least as relevant as high single-filament strength [14], [15].

Most studies on accelerated PAN conversion focus on fiber-level relationships between processing, structure, and properties, while the effect of defined processing parameters on the mechanical response of the resulting composite laminates remains less frequently addressed. In particular, studies that trace industrially relevant carbonization rates of large-tow fibers through to composite-level failure behavior are scarce. This gap is critical because composite design is not governed by fiber tensile properties alone. Under transverse compression and in-plane shear, matrix-dominated deformation, fiber-matrix interaction, and inter-fiber failure can strongly influence the load-bearing capacity of unidirectional laminates. Biaxial loading is therefore especially relevant for assessing whether changes induced during carbonization are reflected in the structural performance of the composite. Combined (σ_2, τ_{21}) loading can cause non-linear stress redistribution and changes in inter-fiber failure mode, making uniaxial properties alone insufficient for evaluating failure behavior under realistic multiaxial stress states [16]. Against this background, the present work investigates how carbonization rate and the resulting fiber properties influence the biaxial mechanical response of corresponding carbon fiber composites. By using industrially relevant processing rates for a 50k tow and evaluating the resulting composites under combined transverse compression and shear, this study establishes a direct link between carbonization conditions and composite-level performance.

2 Materials and methods

2.1 *Specimen preparation and testing*

Carbon fiber reinforced polymer (CFRP) laminates were manufactured by filament winding using three carbon fiber variants, each produced with a different carbonization rate. To this end, a large tow (50 k) commercial PAN-precursor, was processed unaltered using the carbon fiber pilot scale line at Carbon Nexus (Deakin University, Australia) [17], [18]. The PAN-precursor was stabilized, using four center-to-ends oxidation ovens, for a total residence time of 72 min, at temperatures ranging from 220 to 250 °C, and with tension in the range of 6,500 to 8,500 cN. Following stabilization, the tows were collected and, at different rates, individually passed through low-temperature (LT) carbonization at temperatures between 400 and 800 °C with a constant tension of 4,500 cN as well as high-temperature (HT) carbonization at temperatures between 1,100 and 1,400 °C with a constant tension of 7,000 cN. The various processing rates during LT- and HT-carbonization were selected to represent a broad, industrially relevant processing window and resulted in residence times of 15, 5 and 2.5 min, referred to as slow, medium, and fast. After HT-carbonization, an additional tow collection was performed to ensure consistent subsequent electrolytic surface treatment and epoxy-based sizing between tows carbonized at different rates. In this context, the line speed matched that of stabilization, resulting in a residence time of 6 min each. Figure 1 and Table 1 summarize the fiber properties achieved. A detailed description of the fiber manufacturing process, including the resulting fiber properties and microstructure, will be reported in a separate publication. Therefore, the present study focuses on the composite-level biaxial response and discusses the observed differences in relation to the applied carbonization rates.

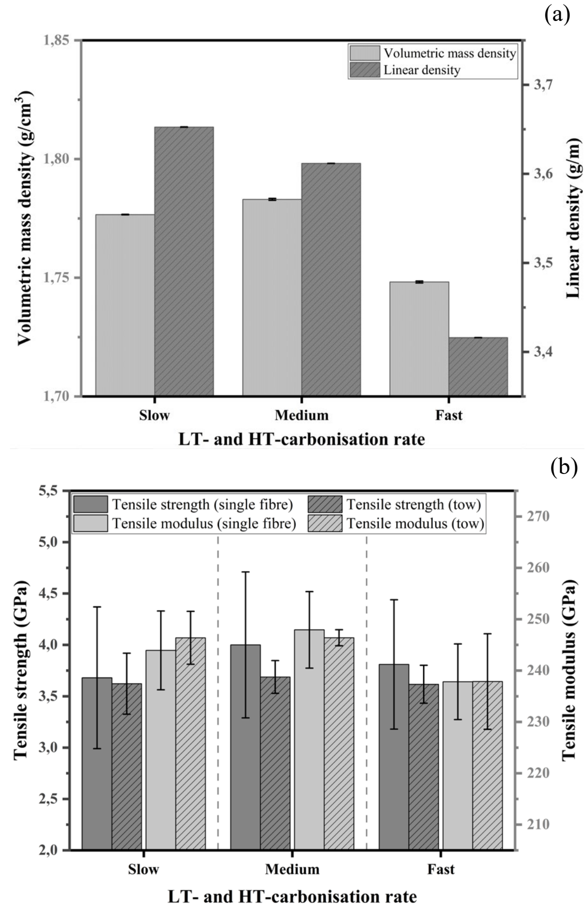

Figure 1: Volumetric mass and linear density (a) as well as mechanical properties determined by single-fiber and tow testing (b) of PAN-fibers after LT- and HT-carbonization at varied residence times.

Table 1: Testing results of carbon fibers carbonized at different rates (values are given as mean ± standard deviation).

	Fiber type		
	Slow	***Medium***	***Fast***
Tensile strength [GPa]	3.62 ± 0.30	3.69 ± 0.16	3.62 ± 0.18
Tensile modulus [GPa]	246.38 ± 5.16	246.40 ± 1.57	237.87 ± 9.30

The produced carbon fibers were wound in a near-0° winding pattern onto 40 x 40 x 5.5 cm rectangular winding mandrels using a Bolenz & Schäfer FWA 2/4/1 filament winding machine. In-line impregnation was achieved via a resin bath, with the resin system consisting of EPIKOTE™ Resin MGS RIMR 935 and EPIKURE™ Curing Agent MGS RIMH 937, mixed at a mass ratio of 100:38. After wet winding of four layers, the entire winding mandrel was removed and the laminate was consolidated by vacuum bagging using the following stack-up on each side: winding body, Polytetrafluoroethylene (PTFE, Teflon) release film, deposited carbon fibers, peel ply, perforated release film, second peel ply, perforated metal plate to promote uniform pressure distribution, breather fleece, and vacuum bag. The assembly was evacuated for 16 h and subsequently cured at 100 °C for 1.5 h. After full cure, the laminate was demolded by cutting along the shorter edge and separating it from the mandrel. The fiber mass fraction was determined by microwave ashing and was comparable for all laminates, with an average value of 69.2 ± 1.1 wt.%. Test specimens were then machined to the final geometry using a high-precision DATRON neo CNC milling machine, ensuring uniform dimensions and clean, parallel edges.

Biaxial characterization was performed according to Svidler *et al.,* using a new fixed-clamped Iosipescu concept [16]. Here, a combined in-plane stress state (σ_2, τ_{21}) is generated in the notch region by superimposing a transverse normal load with the conventional Iosipescu shear loading. The methodology follows the principle that a combined tension or compression and shear stress state can be produced in a firmly clamped Iosipescu specimen. For this purpose, the unloaded specimen areas are rigidly restrained, forcing stress concentration and controlled failure localization into the notch region. This stress and strain localization was previously validated for the same specimen geometry and test setup by finite element simulations and GOM ATOS measurements [16]. In this configuration, the biaxial loading condition can be described by a distortion ratio ($\Omega_\varepsilon = \varepsilon_2/\gamma_{21}$) and the corresponding stress ratio ($\Omega_\sigma = \sigma_2/\tau_{21}$) [16]. In the present work, the actuators were controlled to impose a fixed distortion ratio of $\Omega_\varepsilon = -1$ between the transverse normal strain and the in-plane shear strain. For an undamaged linear-elastic response, this loading path corresponds approximately to a stress ratio of $\Omega_\sigma \approx -1$. It therefore represents a combined transverse-compression and transverse-parallel-shear loading state with nominally equal absolute values of normal and shear stress ($\sigma_2 \approx -\tau_{21}$). The resulting stress ratio was subsequently evaluated from the recorded normal and shear force signals. The loading case, associated with a nominal stress ratio ($\Omega_\sigma \approx -1$) was selected for three reasons:

First, this represents a practically relevant mixed (σ_2, τ_{21}) stress state for UD-reinforced composites. It combines shear-driven damage with a compressive normal component that alters crack growth and frictional sliding along potential fracture planes. The underlying study explicitly discusses that transverse compression and transverse parallel shear have a stabilizing influence compared with transverse tension-shear loading. At the same time, it changes the shear-stress direction and fracture development in the measurement range.

Secondly, for the present material set, the loading case with a nominal stress ratio of $\Omega_\sigma \approx -1$ was expected to provide enhanced differentiation between fiber variants. This loading condition combines transverse compression $R_\perp^{(-)}$ and transverse-parallel shear $R_{\perp\parallel}$, making the response sensitive to both shear damage and splitting behavior. Compared with load cases dominated mainly by matrix cracking, this mixed stress state is expected to involve stronger load sharing through the fibers [19]. Differences introduced by the varied fiber carbonization conditions can therefore become visible in the measured peak stresses and fracture characteristics. In addition, transverse compression can suppress tensile crack opening and promote frictional sliding along developing fracture planes, further increasing the relevance of fiber network stability for the failure [19].

Thirdly, the stress combination (σ_2, τ_{21}) is particularly relevant for the verification of advanced, physically based failure criteria for fiber-reinforced composites. Failure under this mixed transverse compression-transverse parallel shear state delivers not only a characteristic point on the fracture curve but also the corresponding fracture-plane angle θ_{fp}.

During testing, forces in both axes were increased quasi-statically under displacement control while maintaining the targeted distortion ratio of $\Omega_\varepsilon = -1$ until abrupt load drop and global specimen failure. In analogy to the reference work, the (σ_2, τ_{21}) curves can exhibit a slightly undulating progression attributable to friction effects in the mechanical transmission of applied forces, therefore, smoothing by quadratic approximation was used for graphical clarity, whereas peak stresses defining failure were evaluated consistently from the recorded signals [16]. Local deformation in the notch region was monitored using strain gauges applied on both specimen faces (±45° rosette for shear strain and a longitudinal gauge aligned with the normal-loading axis). To guarantee stable signals, proper surface preparation, adhesive curing, and lead wire protection were ensured. The strain gauges enabled simultaneous capture of γ_{21} and ε_2 as well as verification of the intended combined loading condition. In total, seven specimens were tested per fiber type. Outliers were identified using the 1.5 × interquartile range criterion and excluded from the evaluation, affecting at most one specimen per test series. After testing, fracture surfaces and damage patterns were documented using a ZEISS Smartzoom 5 digital microscope, providing high-resolution optical fractography to support failure mode classification and to correlate macroscopic fracture appearance with the measured peak stresses under the nominal ($\Omega_\sigma \approx -1$) loading condition.

The transverse compressive strength required for the calculation of the fracture angle was determined by compression tests in accordance with DIN EN ISO 14126 using a Zwick Z250 universal testing machine. For each fiber type, five specimens were tested, and the resulting mean values were used for evaluation.

2.2 *Improved failure analysis of fiber-reinforced composites*

To interpret the differences in failure behavior between the fibers produced at varying carbonization rates, the biaxial stress results were analyzed using the advanced inter-fiber failure (IFF) concept introduced by Puck [19]. The fracture conditions for the different fracture modes A, B, and C, illustrated in Figure 2, are defined by Equations (1), (2), and (3).

For Mode A:

$$\sqrt{\left(\frac{\tau_{21}}{R_{\perp\parallel}}\right)^2 + \left(1 - p_{\perp\parallel}^{(+)} \frac{R_\perp^{(+)}}{R_{\perp\parallel}}\right)^2 \left(\frac{\sigma_2}{R_\perp^{(+)}}\right)^2} + p_{\perp\parallel}^{(+)} \frac{\sigma_2}{R_{\perp\parallel}} = 1 \tag{1}$$

For Mode B:

$$\frac{1}{R_{\perp\parallel}}\left(\sqrt{\tau_{21}^2 + \left(p_{\perp\parallel}^{(-)}\sigma_2\right)^2} + p_{\perp\parallel}^{(-)}\sigma_2\right) = 1 \tag{2}$$

For Mode C:

$$\left[\left(\frac{\tau_{21}}{2\left(1+p_{\perp\perp}^{(-)}\right)R_{\perp\parallel}}\right)^2 + \left(\frac{\sigma_2}{R_\perp^{(-)}}\right)^2\right]\frac{R_\perp^{(-)}}{(-\sigma_2)} = 1 \tag{3}$$

$R_\perp^{(+)}$ denotes the transverse tensile strength, $R_\perp^{(-)}$ the transverse compressive strength, and $R_{\perp\parallel}$ the transverse-parallel shear strength. $p_{\perp\parallel}^{(+)}$ and $p_{\perp\perp}^{(-)}$ are the corresponding inclination parameters of the Puck criterion [19].

The IFF concept is often illustrated as an interaction curve in the σ_2, τ_{21} plane, as shown in Figure 2. Under compressive σ_2 and shear τ_{21} load, the failure curve lies on the left side of the diagram (Mode B/C), where the dominant mechanisms progressively shift from shear-dominated fracture to splitting-dominated fracture as the fracture-plane orientation rotates and the propensity for fiber-parallel cracking increases. The fracture-plane angle characterized as θ_{fp} and shown in Figure 2 was evaluated in accordance with the recommended IFF conditions using Equation (3) corresponding to Mode C for the investigated (σ_2, τ_{21}) loading case.

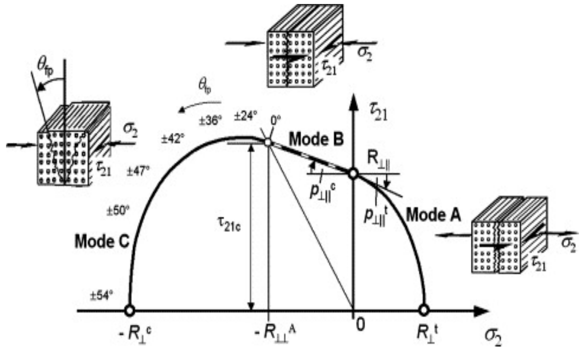

Figure 2: Predicted fracture curve from Puck's inter-fiber fracture criterion [20].

In Puck's concept, IFF occurs on an inclined plane that is obtained by rotating the transverse material axes about the fiber direction, the rotation angle θ_{fp} is chosen such that the stress exposure of this action plane is maximized. For general multiaxial loading, this requires a numerical search over all admissible action-plane orientations, based on the transformed normal and shear stresses. For the present biaxial loading path, however, the stress state at failure lies in the transverse compression - transverse parallel in-plane shear region, where Puck provides an analytical expression for the fracture-plane angle. In this regime (Mode C), the normal stress on the fracture plane is related to the applied transverse stress σ_2 as given by Equation (4).

$$\sigma_{\mathrm{n}}\left(\theta_{\mathrm{fp}}\right) = \sigma_2 \cos^2\left(\theta_{\mathrm{fp}}\right) = -R_{\perp\perp}^{\mathrm{A}} \tag{4}$$

Here, σ_{n} is the normal stress on the fracture plane and $R_{\perp\perp}^{\mathrm{A}}$ is the characteristic breaking resistance on action plane A. Rearranging Equation (4) yields the fracture-plane angle given in Equation (5).

$$\theta_{\mathrm{fp}} = \arccos \sqrt{\frac{R_{\perp\perp}^{\mathrm{A}}}{-\sigma_2}} \tag{5}$$

This explicitly links the fracture orientation to the breaking resistance and the applied transverse compressive stress at failure. The quantity $R_{\perp\perp}^{\mathrm{A}}$ is in turn obtained from the transverse compressive strength $R_{\perp}^{(-)}$ and the inclination parameter $p_{\perp\perp}^{(-)}$ of Puck's IFF criterion according to Equation (6).

$$R_{\perp\perp}^{\mathrm{A}} = \frac{R_{\perp}^{(-)}}{2\left(1+p_{\perp\perp}^{(-)}\right)} \tag{6}$$

In the present evaluation, the transverse compressive strength $R_{\perp}^{(-)}$ was derived from the experimental compression test results summarized in Table 2. The inclination parameter $p_{\perp\perp}^{(-)}$ should ideally be identified from combined stress states. Puck recommends $p_{\perp\perp}^{(-)} = 0.15$ as an initial estimate if no material-specific calibration data are available [19]. In the present study, $p_{\perp\perp}^{(-)} \approx 0.53$ was determined based on laminates with slow carbonized fibers. For the subsequent evaluation of all laminates, a rounded value of $p_{\perp\perp}^{(-)} = 0.50$ was adopted. The influence of this assumption can be illustrated by a brief sensitivity analysis: for $R_{\perp}^{(-)} = 100$ MPa and $\sigma_2 = -80\ MPa$, the predicted Mode C fracture angle increases from 42.5° for $p_{\perp\perp}^{(-)} = 0.15$ to 49.8° for $p_{\perp\perp}^{(-)} = 0.50$. However, the relative trend between the laminates investigated remains unchanged. For each measured failure point $\left(\sigma_{2,\mathrm{f}}, \tau_{21,\mathrm{f}}\right)$, Eqs. (5) and (6) were used to calculate the theoretical fracture-plane angle θ_{fp}, which was then compared with the experimentally measured fracture angles to assess the suitability of the Puck-type description for the present material system.

3 Results and discussion

Biaxial testing was conducted using the previously described fixed-clamped Iosipescu-based setup [16]. The tests followed a loading path with a nominal stress ratio of $\Omega_\sigma = \sigma_2/\tau_{21} \approx -1$, corresponding to a combined transverse compressive stress $\sigma_2 < 0$ superimposed with in-plane shear stress $\tau_{21} > 0$ of equal nominal magnitude. Although the actuators were controlled to impose a fixed distortion ratio of $\Omega_\varepsilon = \varepsilon_2/\gamma_{21} = -1$, the measured trajectories in the σ_2 versus τ_{21} plane are clearly nonlinear as a result of stiffness degradation due to progressive damage. As total failure is approached, the actual stress ratio (Ω_σ) departs from its nominal value. The load path bends toward the σ_2 axis, indicating an increasing dominance of transverse compression. Locally, the instantaneous stress ratio therefore approaches values closer to $\Omega_\sigma \approx -2$.

The measured peak stresses showed a similar trend among the three laminates as observed in the fiber tensile tests and transverse compression tests (Table 2 and 3). Specimens produced from carbon fibers of the slow carbonization rate reached the highest shear stress $\tau_{21,\mathrm{f}} = 33.39$ MPa. However, their compressive stress $\sigma_{2,\mathrm{f}} = -82.06$ MPa was slightly lower than that of specimens containing fibers carbonized at a medium rate ($\sigma_{2,\mathrm{f}} = -82.74$ MPa). Nevertheless, failure at a lower shear stress of $\tau_{21,\mathrm{f}} = 30.80$ MPa suggested that the shear transfer and resistance against shear-driven damage accumulation were reduced with a higher carbonization rate. Specimens with the fast carbonized fibers were inferior to both other variants, failing at $\sigma_{2,\mathrm{f}} = -73.71$ MPa and $\tau_{21,\mathrm{f}} = 29.21$ MPa, which indicated an earlier onset of damage localization and a reduced ability to sustain coupled compression-shear loading (Table 3). Fracture surface inspection revealed a systematic change in failure morphology across the three variants. Specimens reinforced with slowly carbonized fibers showed predominantly shear-dominated failure in the notch region.

Similar shear-dominated features have been reported under purely compressive loading, despite differing fiber orientations [21], [22]. Specimens with fibers carbonized at medium rate exhibited a mixed shear-splitting mode, characterized by inclined shear fracture combined with a tendency toward splitting.

In contrast, specimens with fast carbonized fibers failed predominantly by splitting, with crack propagation following the visible fiber bundles (Figure 3). This ranking aligns well with the measured strength hierarchy, since the transition from shear-dominated to splitting generally corresponds to a reduced achievable shear stress at failure, as splitting provides a preferential damage path that rapidly reduces the shear-carrying ligament. A comparable sensitivity of the dominant failure mode has been reported for laminated plates depending on the compression-shear load ratio, where a shift between buckling and stress-induced failure was observed [23]. This highlights that the dominant failure mode is governed by the applied loading state as well as the fiber quality, which in turn results from the manufacturing conditions.

Table 2: Compression test results of CFRP samples manufactured from CF carbonized at different rates.

	Samples based on fiber type		
	Slow	***Medium***	***Fast***
Transverse compressive strength $R_{\perp}^{(-)}$ [MPa]	104.14 ± 4.21	101.29 ± 4.25	87.99 ± 4.15

Table 3: Biaxial testing results of CFRP Iosipescu samples manufactured from CF carbonized at different rates.

	Samples based on fiber type		
	Slow	***Medium***	***Fast***
Compressive stress σ_2 [MPa]	-82.06 ± 5.15	-82.74 ± 2.50	-73.71 ± 1.55
Shear stress τ_{21} [MPa]	33.39 ± 2.86	30.80 ± 1.78	29.21 ± 1.55
Measured average fracture angle θ_{fp} [°]	49.86 ± 1.77	53.00 ± 4.43	53.71 ± 4.42
Calculated average fracture angle θ_{fp} [°]	49.35 ± 1.53	50.28 ± 0.70	50.88 ± 0.50

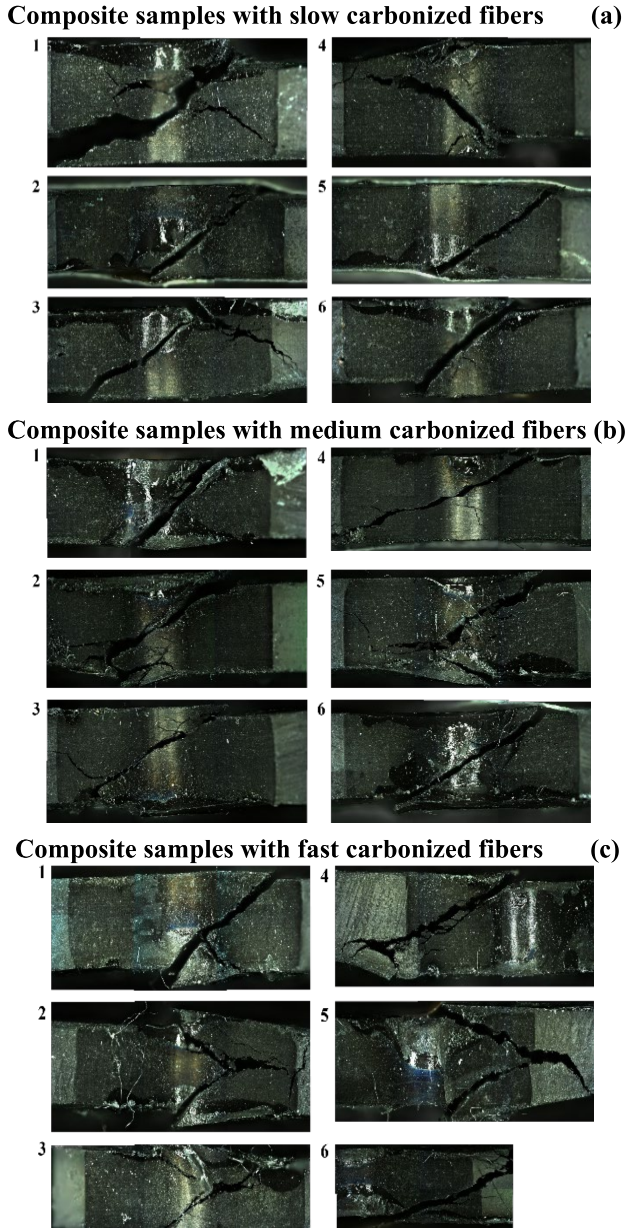

Figure 3: Failure of samples produced with slow (a), medium (b) and fast (c) carbonized fibers under biaxial loading.

The measured fracture angles lie close to those reported for uniaxial compression [24], which is reasonable given the compression-shear load ratio applied [23], [24]. The fracture angles agreed reasonably well with the values calculated using the adopted inclination parameter $p_{\perp\perp}^{(-)}$=0.50 (Table 3). Overall, the calculations predicted a 3.0 % increase in θ_{fp} from fast to slow carbonized fibers, while the experiments showed an increase of 7.2 %.

Therefore, measured fracture angles appeared to follow the same trend, although the interpretation was complicated by high standard deviation and complex fracture patterns.

Deviations may be caused by defects or influences that are not fully captured by the idealized, homogeneous action-plane approach. In particular, specimen geometry and notch configuration can generate local stress states in the gauge region that deviate from the simplified (σ_2, τ_{21}) plane assumption. Since the same matrix system and composite manufacturing conditions were used for all laminates, matrix-related effects were assumed to remain constant; however, possible differences in fiber-matrix interaction caused by the varied carbonization rates may additionally affect the shear-dominated failure response.

Finally, frictional and boundary effects in the clamped notch specimen, together with nonlinearities prior to peak load, can alter the effective load transfer and lead to a fracture path with a slightly different apparent inclination [20], [25]. This provides a physically consistent explanation for both the small discrepancy between measured and calculated fracture angles as well as the standard deviation.

The combined evolution of fracture angles and fracture morphology confirms a transition from shear-dominated failure for laminates with slow carbonized fibers to mixed shear-splitting failure and predominantly splitting-dominated failure for laminates with fast carbonized fibers. This transition is accompanied by increasing fracture angles, while specimens containing fast carbonized fibers showed lowest peak stresses. Accordingly, larger fracture angles do not indicate higher load-bearing capacity, but rather a stronger contribution of splitting-related damage. The results show that the effect of carbonization rate must be assessed by both peak stresses and the associated failure mode.

Prior to ultimate specimen failure, the recorded response curve of some specimens exhibited a characteristic increase in load-bearing capacity, although the final stress levels remained comparable. This behavior is also reflected in the averaged biaxial stress curves (Figure 4). The observed pre-failure strengthening may be related to progressive matrix shear deformation, local damage redistribution and minor fiber reorientation or waviness under combined compression-shear loading. Such mechanisms are consistent with the known sensitivity of UD composites to local fiber waviness and matrix shear deformation under compression-dominated failure [26].

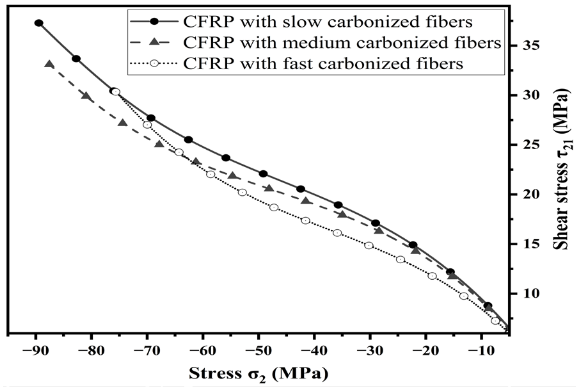

Figure 4: Averaged (σ_2, τ_{21}) curves for composites reinforced with carbonized fibers at slow, medium, and fast rates.

This is consistent with the initial material ranking, the results derived from the compression tests, as well as with the measured peak stresses and observed failure behavior in the biaxial tests. Overall, the curves, obtained by averaging over the maximum x-range, confirm the same general material ranking. Laminates containing slower carbonized fibers showed higher biaxial load-bearing capacity than laminates with faster carbonized fibers.

4 Conclusion

This work reviewed key strategies for improving the efficiency of PAN-based carbon fiber manufacturing and experimentally examined an accelerated carbonization approach by varying carbonization rates. While all fibers showed similar tensile properties and met typical automotive target values [27], [28], biaxial compression-shear tests along nominal stress ratio of $\Omega_\sigma \approx$ -1 revealed differences at the composite level.

Composites reinforced with slowly carbonized fibers reached the highest shear peak stresses and showed predominantly shear-dominated failure. Specimens with fibers carbonized at medium rate reached the highest transverse compressive peak stresses and exhibited a mixed shear and splitting failure mode. In contrast, specimens with fast carbonized fibers showed the lowest overall biaxial performance and failed mainly by splitting. However, the reduced mechanical performance of composites with fast carbonized fibers must be weighed against the increased productivity enabled by accelerated carbonization, particularly if the resulting properties are still sufficient for a specific application.

The transition from shear-dominated to splitting-dominated failure and the systematically changing fracture-plane angles demonstrate that fibers with similar tensile properties can lead to distinct multiaxial composite responses when produced under different carbonization schedules. Thus, the study provides a direct process to composite perspective and supports the definition of application-oriented carbonization rates. Further work will extend the mechanical database to additional loading cases and fracture toughness properties. The resulting data will be used to develop material cards for simulation-based component design and enable targeted prediction of composite performance already during the selection of fiber production process parameters.

Nomenclature

Parameter Notation	Parameter Definition	Unit
ε_2	Transverse normal strain perpendicular to the fiber direction (lamina 2-direction)	-
γ_{21}	Transverse-parallel shear strain (2-1 plane)	-
Ω_ε	Distortion ratio between transverse normal and transverse-parallel shear strain	-
σ_2	Transverse normal stress perpendicular to the fiber direction (lamina 2-direction)	MPa
τ_{21}	In-plane transverse-parallel shear stress (2-1 plane)	MPa
σ_n	Normal stress acting on the fracture plane used in the Puck IFF criterion	MPa
$\sigma_{2,f}$	Transverse normal stress in the biaxial test at failure (lamina 2-direction)	MPa
$\tau_{21,f}$	In-plane transverse-parallel shear stress in the biaxial test at failure (2-1 plane)	MPa
Ω_σ	Stress ratio between transverse normal and transverse-parallel shear stress	-
θ_{fp}	Fracture-plane angle in the Puck IFF concept	°
$R_\perp^{(+)}$	Transverse tensile strength of the lamina (IFF strength under normal tensile stress in lamina 2-direction).	MPa
$R_\perp^{(-)}$	Transverse compressive strength of the lamina (IFF strength under normal compressive stress in lamina 2-direction)	MPa
$R_{\perp\parallel}$	Transverse-parallel shear strength of the lamina (2-1 plane)	MPa
$R_{\perp\perp}^{A}$	Characteristic normal stress resistance on action plane A in transverse compression	MPa
$p_{\perp\perp}^{(-)}$	Inclination parameter of the Puck IFF criterion describing the influence of normal compressive stress on the fracture plane	-
$p_{\perp\parallel}^{(+)}$	Inclination parameter of the Puck IFF criterion describing the influence of normal tensile stress on the fracture plane under combined transverse tension and transverse-parallel shear	-
$p_{\perp\parallel}^{(-)}$	Inclination parameter of the Puck IFF criterion describing the influence of normal compressive stress on the fracture plane under combined transverse compression and transverse-parallel shear	-

Acknowledgments

The authors gratefully acknowledge financial support from Deakin University, Australia, through the Deakin University DUPR scholarship. The authors also thank the Institute for Frontier Materials (Deakin University), the ARC Centre for Future Fibers (IH210100023) and the Department of Lightweight Structures and Polymer Technology (University of Technology Chemnitz) for use of facilities and providing access to equipment and infrastructure. The operations teams are thanked for their valuable support during the trials.

Author Contributions

M.K.: conceptualization, investigation, methodology, formal analysis, data curation, writing an original draft, review and editing; M.M.: methodology, manufacturing process input, writing, review and editing; R.V.: supervision, methodology, failure assessment, formal analysis, review and editing; R.S.: methodology, experimental design, visualization, validation, formal analysis, writing, review and editing; L.K.: supervision, methodology, failure characterization, calculations, writing, review and editing; C.C.: supervision, methodology, evaluation, formal analysis, writing, review and editing.

Conflicts of Interest

The authors declare no conflict of interest.

Declaration of AI tools

During the preparation of this work, GPT-4.5 was used to improve the language, grammar, and readability of the manuscript. After using this tool, the authors reviewed and edited the content as needed. The authors take full responsibility for the content of the published article.

References

[1] M. A. Stróżyk et al., “Decreasing the environmental impact of carbon fibre production via microwave carbonisation enabled by self-assembled nanostructured coatings,” *Advanced Composites and Hybrid Materials*, vol. 7, no. 2, pp. 39, Feb. 2024, doi: 10.1007/s42114-024-00853-2.

[2] H. Chen, H. P. H. Liddell, A. A. Ogale, Z. C. Miao, M. W. Ijeoma, and M. Carbajales-Dale,

"A critical review and meta-analysis of energy demand, carbon footprint, and other environmental impacts from carbon fiber manufacturing," *Resources, Conservation and Recycling*, vol. 219, Art. no. 108302, Jun. 2025, doi: 10.1016/j.resconrec.2025.108302.

[3] A. Dér et al., "Modelling and analysis of the energy intensity in polyacrylonitrile (PAN) precursor and carbon fibre manufacturing," *Journal of Cleaner Production*, vol. 303, Art. no. 127105, Jun. 2021, doi: 10.1016/j.jclepro.2021.127105.

[4] H. Khayyam et al., "Improving energy efficiency of carbon fiber manufacturing through waste heat recovery: A circular economy approach with machine learning," *Energy*, vol. 225, Art. no. 120113, Jun. 2021, doi: 10.1016/j.energy.2021. 120113.

[5] J. Wolf et al., "Thermomechanical modeling of the stabilization process for carbon fiber production," *Chemical Engineering & Technology*, vol. 46, no. 11, pp. 2442-2447, Nov. 2023, doi: 10.1002/ceat.202300316.

[6] K. Sakamoto, K. Kawajiri, H. Hatori, and K. Tahara, "Impact of the manufacturing processes of aromatic-polymer-based carbon fiber on life cycle greenhouse gas emissions," *Sustainability*, vol. 14, no. 6, Art. no. 3541, Mar. 2022, doi: 10.3390/su14063541.

[7] H.-M. Park et al., "Implementation of regenerative thermal oxidation device based on high-heating device for low-emission combustion," *Energies*, vol. 17, no. 20, Art. no. 5182, Oct. 2024, doi: 10.3390/en17205182.

[8] J. Kaur, K. Millington, and S. Smith, "Producing high-quality precursor polymer and fibers to achieve theoretical strength in carbon fibers: A review," *Journal of Applied Polymer Science*, vol. 133, no. 38, Art. no. 43963, Sep. 2016, doi: 10.1002/app.43963.

[9] T. Morishita et al., "Carbon fibre production using an ecofriendly water-soluble precursor," *Nature Communications*, vol. 16, no. 1, Art. no. 4614, May 2025, doi: 10.1038/s41467-025-59841-9.

[10] R. Norris, C. Eberle, F. Paulauskas, V. Kunc, K. Yarborough, and N. Vashisth, "Melt-spun PAN precursor for cost-effective carbon fibers in high pressure compressed gas tankage," Oak Ridge National Lab. (ORNL), Oak Ridge, TN, USA, Tech. Rep. ORNL/TM-2022/2761, Dec. 2022, doi: 10.2172/2315608.

[11] H.-C. Hsu, H.-W. Chao, W.-C. Huang, and T.-H. Chang, "Stabilization of polyacrylonitrile-based fiber with a quasi-traveling microwave applicator," *Scientific Reports*, vol. 14, no. 1, Art. no. 18718, Aug. 2024, doi: 10.1038/s41598-024-69641-8.

[12] S.-Y. Kim, S. Y. Kim, S. Lee, S. Jo, Y.-H. Im, and H.-S. Lee, "Microwave plasma carbonization for the fabrication of polyacrylonitrile-based carbon fiber," *Polymer*, vol. 56, pp. 590-595, Jan. 2015, doi: 10.1016/j.polymer.2014.11.034.

[13] Y. Sha et al., "Laser induced graphitization of PAN-based carbon fibers," *RSC Advances*, vol. 8, no. 21, pp. 11543-11550, Mar. 2018, doi: 10.1039/c8ra00497h.

[14] A. Maier and L. Kroll, "Experimental investigation of automotive component in hybrid fibre reinforced thermoplastic design," *Technologies for Lightweight Structures (TLS)*, vol. 5, pp. 96-103, Mar. 2022, doi: 10.21935/tls.v5i1.161.

[15] C. Zopp et al., "Manufacturing, interfacial adhesion and mechanical investigations of inverse hybrid composite laminates: Carbon fibre-reinforced Polyamide-6/Aluminium," *Journal of Materials Research and Technology*, vol. 38, pp. 5186-5194, Sep. 2025, doi: 10.1016/j.jmrt.2025. 08.242.

[16] R. Svidler, R. Rinberg, S. Mueller, L. Kroll, and M. Kroll, "Biaxial testing and failure criterion validation for flax fibre-reinforced plastics using a novel test method," *Composites Part B: Engineering*, vol. 306, Art. no. 112802, Nov. 2025, doi: 10.1016/j.compositesb.2025.112802.

[17] T. Groetsch et al., "Gas emission study of the polyacrylonitrile-based continuous pilot-scale carbon fiber manufacturing process," *Industrial & Engineering Chemistry Research*, vol. 60, no. 48, pp. 17379-17389, Dec. 2021, doi: 10.1021/acs.iecr.1c02253.

[18] S. Nunna et al., "Time dependent structure and property evolution in fibres during continuous carbon fibre manufacturing," *Materials*, vol. 12, no. 7, Art. no. 1069, Apr. 2019, doi: 10.3390/ma12071069.

[19] A. Puck, *Festigkeitsanalyse von Faser-Matrix-Laminaten*, Ed., Munich, Vienna: Carl Hanser Verlag, 1996.

[20] A. Puck and M. Mannigel, "Physically based non-linear stress–strain relations for the inter-fibre fracture analysis of FRP laminates," *Composites Science and Technology*, vol. 67, no. 9, pp. 1955-1964, Jul. 2007, doi: 10.1016/j.compscitech.2006.10.008.

[21] Y. Ma, Y. Li, and L. Liu, "Off-Axis compressive behaviour of fibre reinforced thermoplastic composites," *Materials*, vol. 15, no. 16, Art. no. 5547, Aug. 2022, doi: 10.3390/ma15165547.

[22] S. Krishnappa and S. Gururaja, "Compressive failure mechanisms in unidirectional fiber reinforced polymer composites with embedded wrinkles," Composites Part B: Engineering, vol. 284, Art. no. 111688, Sep. 2024, doi: 10.1016/j.compositesb.2024.111688.

[23] R. Pianet et al., "Experimental and numerical studies in the failure behavior of CFRP plates under combined compression-shear loading," *Journal of Reinforced Plastics and Composites*, vol. 45, no. 5-6, pp. 1351-1363, Mar. 2026, doi: 10.1177/07316844251322924.

[24] Y. Kumar, M. Rezasefat, Z. Zaiemyekeh, H. Li, P. Dolez, and J. Hogan, "Dynamic In-Plane Compression and Fracture Growth in a Quasi-Isotropic Carbon-Fiber-Reinforced Polymer Composite," *Materials*, vol. 17, no. 24, Art. no. 6296, Dec. 2024, doi: 10.3390/ma17246296.

[25] P. Ballarin, A. Airoldi, P. Aceti, S. Ghiasvand, and G. Sala, "Experimental identification of frictional effects on interlaminar toughness of composite laminates in 4ENF test," *Experimental Mechanics*, vol. 62, no. 7, pp. 1135-1145, Sep. 2022, doi: 10.1007/s11340-022-00860-8.

[26] J. Chen, L. Wan, K. Nelms, G. Allegri, and D. Yang, "Failure analysis of unidirectional CFRP composites with the coupled effects of initial fibre waviness and voids under longitudinal compression," *Composite Structures*, vol. 347, Art. no. 118451, Nov. 2024, doi: 10.1016/j.comp struct.2024.118451.

[27] N. V. Salim, S. Blight, C. Creighton, S. Nunna, S. Atkiss, and J. M. Razal, "The role of tension and temperature for efficient carbonization of polyacrylonitrile fibers: toward low cost carbon fibers," *Industrial & Engineering Chemistry Research*, vol. 57, no. 12, pp. 4268-4276, Mar. 2018, doi: 10.1021/acs.iecr.7b05336.

[28] X. Huang, "Fabrication and properties of carbon fibers," *Materials*, vol. 2, no. 4, pp. 2369–2403, Dec. 2009, doi: 10.3390/ma2042369.